

Chapter 6

Optical diffraction in defect lattices

6.1 Introduction

Optical diffraction is another method to study the structural features of an heterogenous medium. In this chapter, we undertake such a study in the systems described in the previous chapter viz., *TGBs* and tapered lattices. The propagation of light at an angle to the direction of periodic modulation of the index tensor results in diffraction. A plane wavefront incident with the propagation vector (k) perpendicular to the direction of modulation emerges as a corrugated wavefront. This corrugated wavefront gives rise to diffraction. This is also referred to as the phase grating mode. This is the geometry considered throughout this chapter. In the case of *TGB_A*, *TGB_{C_{||}}* and twist tapered lattice, if the linearly polarised incident light has its electric vector perpendicular to the twist axis i.e., $E = E_{\perp}$ at each point, then the light emerges in the same state of polarisation but with different phases at different points. As a result,

we get a corrugated wavefront polarised perpendicular to the twist axis. Hence we find diffraction for this polarisation. For the electric vector parallel to the twist axis i.e., $E = E_{\parallel}$, the structure is optically not heterogenous and hence the emergent wavefront will continue to be a plane wavefront and there will be no diffraction.

In the case of $TGB_{C_{\perp}}$ and splay-bend tapered lattice, for any azimuth of the incident linear vector the medium is periodically heterogenous. Hence we get optical diffraction for all azimuths. However, diffraction in splay-bend tapered lattices is more complicated and will be discussed later in this chapter.

6.2 Theory of optical diffraction

6.2.1 Thin samples

As said earlier, in TGB_A , $TGB_{C_{\parallel}}$ and twist tapered lattices diffraction takes place only for the component of the electric vector perpendicular to the twist axis. A general geometry for diffraction is shown in Figure 6.1. In such cases, if the medium is weakly heterogenous then we can ignore internal optical diffraction. Further we assume that the amplitude of the corrugation of the wavefront is much smaller than the wavelength of corrugation which is assumed to be large compared to the wavelength of light. This is the essence of the generalised Raman-Nath theory (RN) [1]. At any diffraction angle Θ the diffracted amplitude is given by [1] the fourier transform the corrugated emergent vibration i.e.,

$$U(\Theta) = \int_{-\infty}^{\infty} \exp(-i\frac{2\pi z}{\lambda} \sin\Theta) [\exp(i\frac{2\pi t}{\lambda} \mu(z))] dz \quad (6.1)$$

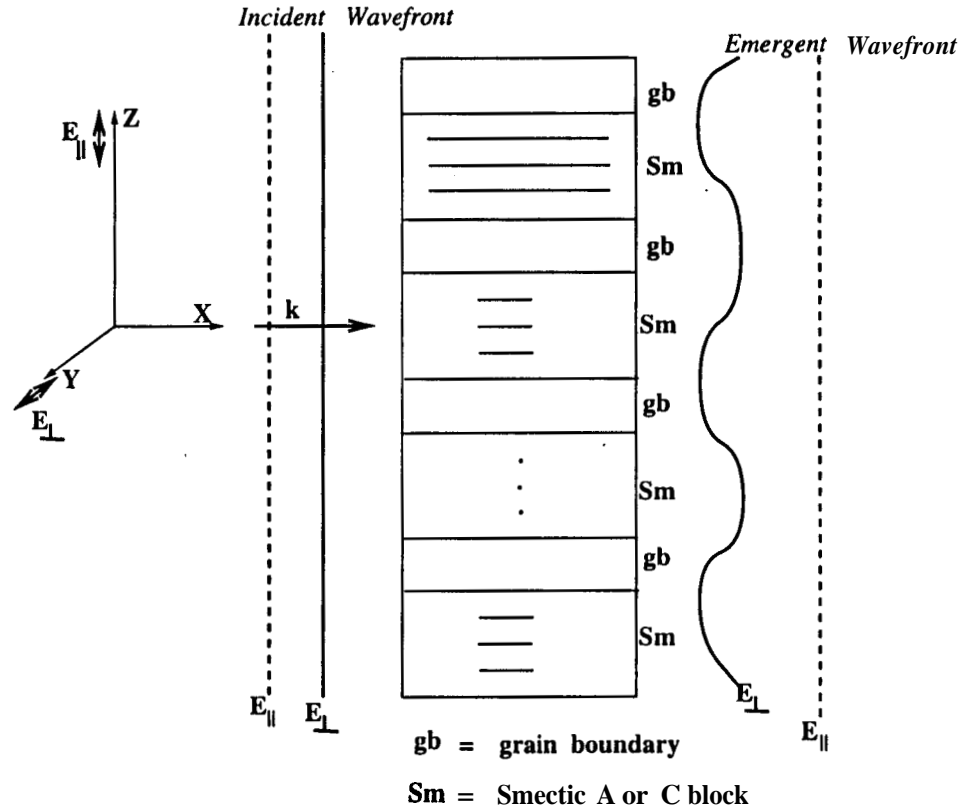


Figure 6.1: The geometry for *diffraction* in TGB_A or $TGB_{C\parallel}$. In a twist tapered lattice the twist axis is again along z . Here the dotted line denotes an incident wavefront with E parallel to the twist axis. The solid **line** is for E *perpendicular* to the twist axis.

where

$$\frac{1}{(\mu(z))^2} = \frac{(\sin(\psi(z)))^2}{\mu_e^2} + \frac{(\cos(\psi(z)))^2}{\mu_o^2} \quad (6.2)$$

Here μ_o and μ_e are the local ordinary and the extraordinary refractive indices, $\psi(z)$ the orientation of the local director with respect to the x axis and t is the sample thickness perpendicular to the direction of propagation. Since $\mu(z)$ is periodic with period $p/2$ we get diffraction peaks at

$$\Theta = \pm \sin^{-1}(2m\lambda/\mu p) \quad (6.3)$$

Here m is an integer. In principle we can experimentally extract $U(\Theta)$ both in amplitude and phase. Then from (6.1) through a Fourier inversion, we can get in principle, $\mu(\mathbf{z})$ or equivalently $\psi(\mathbf{z})$. Hence we can retrieve the director profile in the system.

6.2.2 Thick samples

When the sample is thick, internal diffractions become important and to incorporate this we use the **Rokushima-Yamakita** theory (RY) [2]. Here the medium is sliced into thin slabs and within each slab the Raman-Nath approximation is assumed to be valid. When a plane wavefront enters the first slab it emerges out of it as a corrugated wavefront. In other words, we get the light being diffracted into different orders. When this light enters the next slab each of the diffracted beam undergo further diffraction. Thus finally, in each order of diffraction we have many beams each due to a slab contributing to diffraction. All this will have to be added coherently to get the net diffracted intensity in any desired direction. Hence at any point, we have different components of the electric and magnetic fields, each due to a diffracted beam. Thus, in this theory the \mathbf{E} and \mathbf{H} vectors of the incident plane electromagnetic wave and the components of the dielectric tensor are expressed as Fourier sums with weighted coefficients. The Maxwell's equations in the RY notation become:

$$\frac{d}{dx} f_{\hat{i}} = iC f_{\hat{i}} \quad (6.4)$$

$$f_{\hat{n}} = D f_{\hat{i}} \quad (6.5)$$

$$(6.6)$$

with $\bar{x} = x\omega/c$. Here

$$f_{\hat{i}} = \begin{pmatrix} \tilde{e}_y \\ \tilde{h}_z \\ \tilde{e}_z \\ \tilde{h}_y \end{pmatrix} \quad \text{and} \quad f_{\hat{n}} = \begin{pmatrix} \tilde{e}_x \\ \tilde{h}_x \end{pmatrix}$$

are respectively the tangential and normal components of the fields at the interfaces. Also $\tilde{e}_i = \tilde{e}_i(\bar{x})$ and $\tilde{h}_i = \tilde{h}_i(\bar{x})$ are infinite column matrices with elements $e_{im}(\mathbf{x})$ and $h_{im}(\mathbf{x})$, m being an integer. These elements are the Fourier components of E_i and H_i respectively. The coupling matrices C and D are given by

$$C = \begin{pmatrix} 0 & -1 & 0 & 0 \\ \varepsilon_{yx}\varepsilon_{xx}^{-1}\varepsilon_{xy} - \varepsilon_{yy} + \tilde{q}^2 & 0 & 0 & -\varepsilon_{yx}\varepsilon_{xx}^{-1}\tilde{q} \\ \tilde{q}\varepsilon_{xx}^{-1}\varepsilon_{xy} & 0 & 0 & -\tilde{q}\varepsilon_{xx}^{-1}\tilde{q} + 1 \\ 0 & 0 & \varepsilon_{zz} & 0 \end{pmatrix}$$

$$D = \begin{pmatrix} -\varepsilon_{xx}^{-1}\varepsilon_{xy} & 0 & 0 & \varepsilon_{xx}^{-1}\tilde{q} \\ -\tilde{q} & 0 & 0 & 0 \end{pmatrix}$$

Here

ε_{ij} ($i, j = x, y, z$) are $(2m+1) \times (2m+1)$ sub-matrices with elements

$\varepsilon_{ij, nl} = \varepsilon_{ij, n-l}$, the $(n-l)^{\text{th}}$ Fourier component of ε_{ij}

$$\tilde{q} = \delta_{nl} q_l$$

$$q_l = lq + q_0$$

$$q = 2\pi/p \text{ and } q_o = n_i \sin \beta$$

n_i is the refractive index of the first bounding medium and β is the angle of incidence. The solution to the coupled-wave equations (6.5) and (6.6) essentially reduces to an eigenvalue problem of the matrix C . In terms of f_i ; we define,

$$\mathbf{g} = T^{-1} f_i \quad (6.7)$$

Here T is the transformation matrix which has the eigenvectors of C as its columns. This transforms equation (6.6) to

$$\frac{d}{dx} \mathbf{g} = j C_d \mathbf{g} \quad (6.8)$$

Here C_d is a **diagnol** matrix containing the eigenvalues of C . Equation (6.8) can be solved to get the components of f_i . The characteristic fields corresponding to these solutions have their electric vectors are either in the plane of diffraction (TM) or perpendicular to it (TE). The diffraction has the coupling of these TM and TE modes through C .

6.3 Twist grain boundary smectics

While considering diffraction from $TGBS$, three different structures are considered. TGB_A which is very much like a cholesteric and the two $TGB_{C_{\parallel}}$ and $TGB_{C_{\perp}}$ structures. In $TGB_{C_{\parallel}}$, its two-fold axis parallel to the twist axis is rather optically analogous to TGB_A . The schematic representation of $TGB_{C_{\parallel}}$ and $TGB_{C_{\perp}}$ are shown in Figure 6.2. In TGB_A and $TGB_{C_{\parallel}}$ the director is in the $x - y$ plane and twists about z . In $TGB_{C_{\perp}}$, on the other hand, the director is at an angle with respect to z and precess about it as we go from one smectic block to the next.

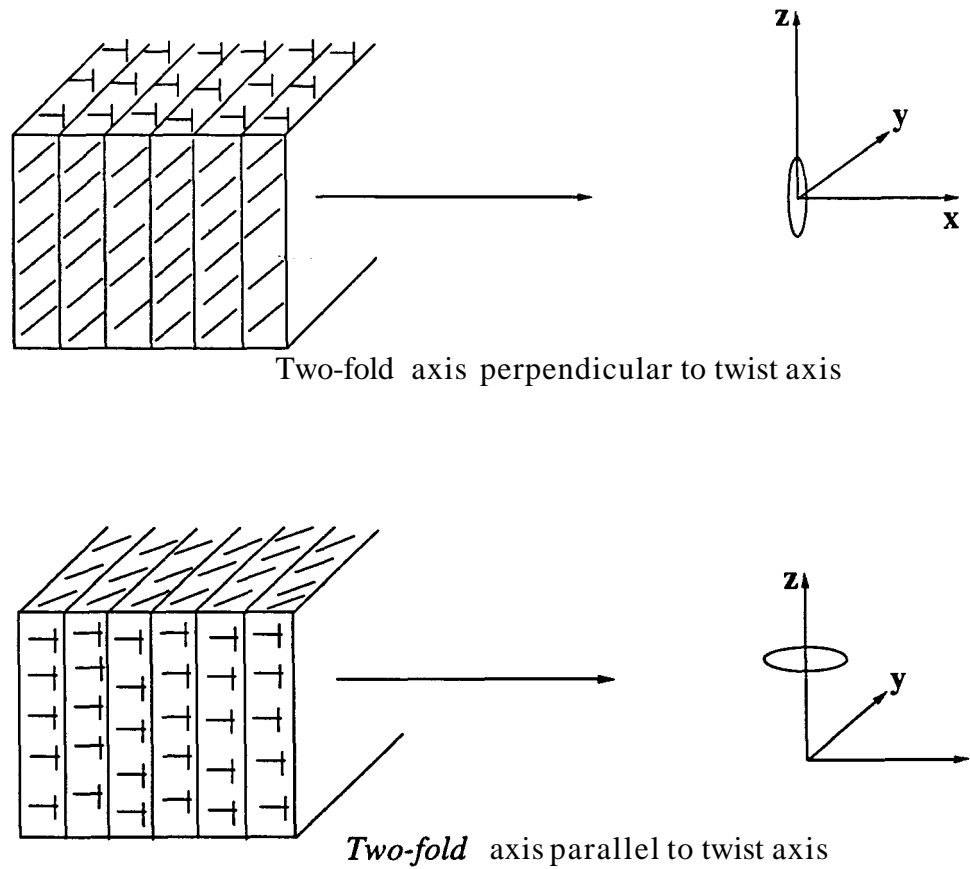


Figure 6.2: Schematic representation of local smectic **blocks** in $TGB_{C_{\perp}}$ and $TGB_{C_{\parallel}}$. z is the twist axis.

Thin Samples

Raman-nath theory which is described before is employed for thin samples of TGB_A and $TGB_{C_{\parallel}}$ for \mathbf{E}_{\perp} polarisation. Both TGB_A and $TGB_{C_{\parallel}}$ have similar diffraction patterns. In principle, it is possible to get the phase of the diffracted beams through an interference or holographic technique. Thus we know the amplitude as well as the phase of the diffracted beams. From Fourier inversion we can get $\mu(z)$ or equivalently $\psi(z)$. From the structure of $TGBS$

it is obvious that $\psi(z)$, the orientation of the local director with respect to the x axis is a constant along z in the smectic blocks and varies with z only in the

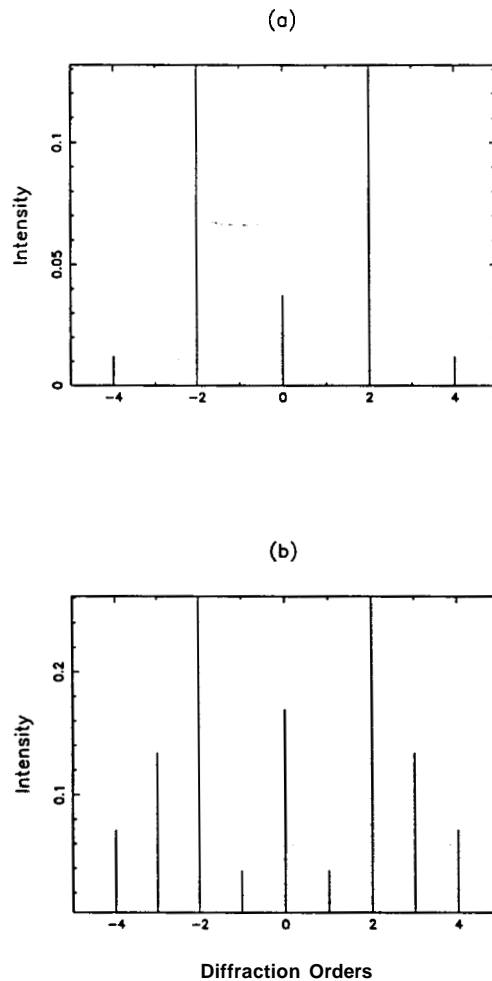


Figure 6.3: A typical *diffraction* pattern for \mathbf{E}_\perp polarization of incident light. (a) TGB_A (or TGB_{C_\parallel}) and (b) TGB_{C_\perp} computed for a sample thickness of 20μ .

grain boundaries. Hence determination of $\psi(z)$ profile leads to an evaluation of the thickness of the smectic block and that of the grain boundary. Also this method will reveal the nature of the director twist present inside the grain boundary.

Thick Samples

Diffraction pattern has been computed for thick samples using the RY theory. In Figure 6.3(a) we give a computed diffraction pattern of TGB_A . An essentially similar pattern is obtained for $TGB_{C_{\parallel}}$. It is seen to be symmetric. It must be remarked that the intensity of any order is a sensitive function of sample thickness. Also in TGB_A or $TGB_{C_{\parallel}}$ for an incident light at any

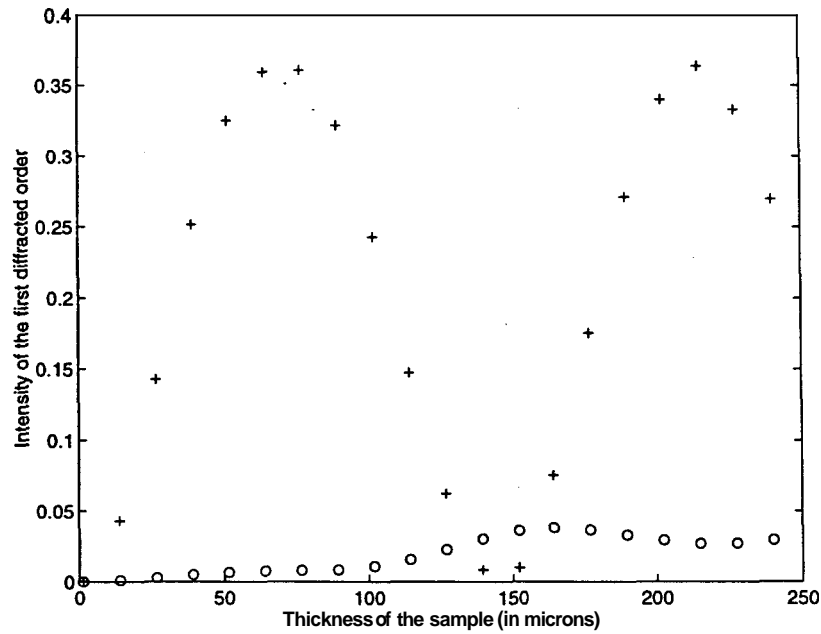


Figure 6.4: $TGB_{C_{\perp}}$: Variation of intensity of first *diffracted* order *with* thickness in E_{\perp} (shown in +) and E_{\parallel} (shown in o) modes for an incident E_{\perp} mode

general azimuth the central order is elliptically polarized while all the higher diffraction orders are nearly linearly polarized perpendicular to the twist axis. As in the case of thin samples, even here optical diffraction takes place when the incident light is polarised with its electric vector perpendicular to the twist axis i.e., E_{\perp} mode. On the other hand no diffraction takes place for incident

light polarized parallel to the twist axis i.e., E_{\parallel} mode.

In $TGB_{C_{\perp}}$ we get diffraction for any azimuth of the linearly polarised incident light. Since the optical period is μp , the pattern has extra orders which happen to be the odd orders of diffraction. In Figure 6.3(b) we give the computed diffraction pattern for $TGB_{C_{\perp}}$ for E_{\perp} mode. In any given order the polarization is dependant on the azimuth of incident polarization and the thickness of the sample. We find, the intensity of the central order in the E_{\perp} mode to be always much higher than the intensity in the E_{\parallel} mode. Thus the central order is nearly always polarised perpendicular to the twist axis i.e., it is of E_{\perp} polarisation. In the first order, for incident E_{\perp} mode, the diffracted intensity in E_{\perp} is always higher than the diffracted intensity in E_{\parallel} mode. However in a narrow range of thickness around 150μ the E_{\parallel} mode intensity of the first diffracted order is greater than that of E_{\perp} mode. This thickness dependance is shown in Figure 6.4. Thus $TGB_{C_{\perp}}$ behaves like chiral smectic C in the diffraction mode [3].

In summary, we cannot differentiate, using diffraction optics, between TGB_A and $TGB_{C_{\parallel}}$. But these two can be differentiated from $TGB_{C_{\perp}}$. It must be noted that in **all** these cases the diffraction pattern is symmetric. We conclude this section with a few remarks. If the structures are incommensurate then they become quaziperiodic. Then it is not possible to work out the diffraction pattern using RY theory. However, we can work out diffraction in thin samples using RN theory. Such a problem has already been addressed to by others in a different system [4, 5]. The important result is that in such structures we get very many diffraction orders and each order will have to be described by a pair of integers. This is also true of TGB_S .

6.4 Tapered Lattice

6.4.1 Twist tapered lattice

In the limit of no damping, the tapered lattice is nothing but a periodic sine or cosine curve associated with a soliton. Then it is similar to a cholesteric

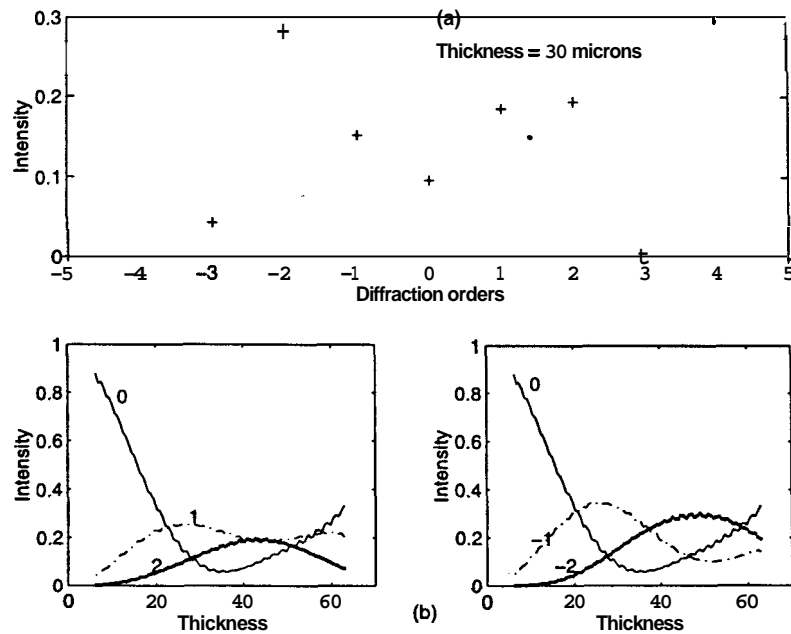


Figure 6.5: *Asymmetric diffraction in a twist tapered lattice for incident E_{\perp} polarisation. (a) Diffraction pattern (b) Thickness dependence in different orders.*

structure. In cholesteric, we get a diffraction pattern that is symmetric. However, in the case of the tapered lattices because of the exponential damping the pattern is very different. To calculate the diffraction pattern of a twist tapered lattice we have made use of the RY theory described earlier. Diffraction of light results only for electric vector perpendicular to the twist axis (E_{\perp}). As already said, the light with electric vector parallel to the twist axis (E_{\parallel}) does

not give rise to any diffraction. Further, for the E_{\perp} polarisation, the direction of normal incidence of light can be at any azimuth with respect to the x axis. The diffraction pattern will be dependant on this azimuth. In this sense these structures are different from TGBS which have a cylindrical symmetry about the twist axis.

In Figure 6.5, the diffraction pattern for E_{\perp} is shown for light incident parallel to the x axis. The pattern is asymmetric. In some thickness range, the intensity of the central order can be much less than the intensity of the other higher diffracted orders. The polarisation of a particular order is a sensitive function of the sample thickness.

6.4.2 Splay-bend tapered lattice

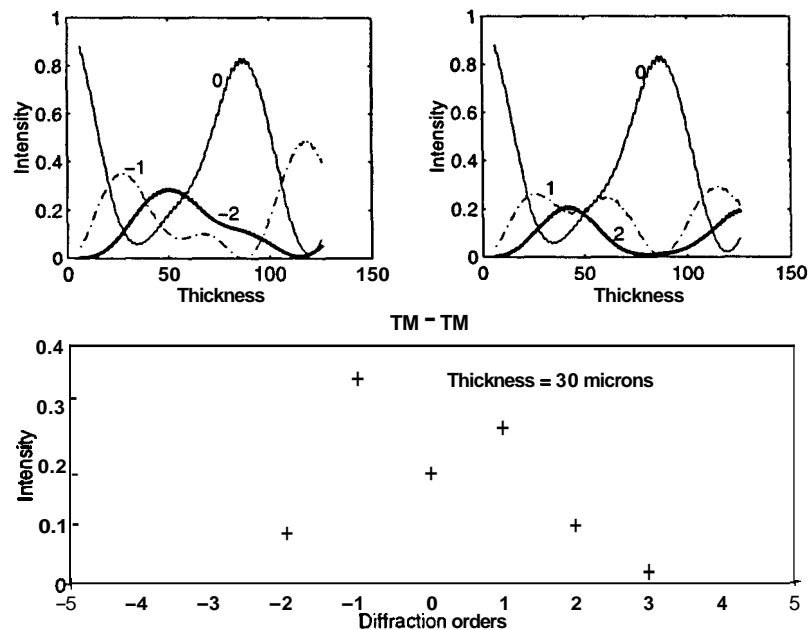


Figure 6.6: Diffraction in a splay-bend *tapered* lattice for a E_{\parallel} polarisation

We consider the modulation to be along the z axis in the xz plane. Diffraction pattern for light incident along y -axis with both for E vector parallel to x axis (E_{\perp}) and parallel to z axis (E_{\parallel}) have been worked out (see Figure 6.7(a)). The pattern for E_{\parallel} polarisation is shown in Figure 6.6. The diffraction pattern is again asymmetric as in the case of the twist tapered lattice. The polarisation of the light in different orders is a sensitive function of the

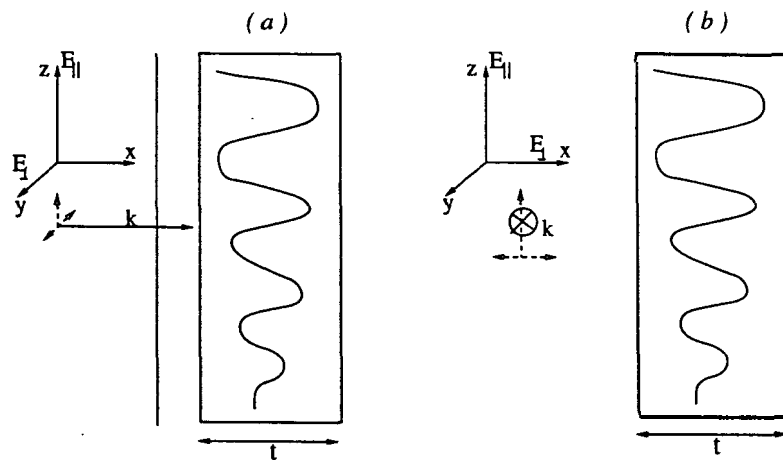


Figure 6.7: *Diffraction geometries for the splay-bend lattice*

thickness of the sample. The central order can be of a lesser intensity than the other orders depending on the sample thickness. The E_{\parallel} polarisation gives rise to strong diffraction while the E_{\perp} gives rise to a weak diffraction only. The different orders are general elliptically polarised. The ellipticity varies with sample thickness.

Contrasting the diffraction features of the twist tapered lattice and the splay bend tapered lattice we see that though both have similar diffraction

features, the strong diffraction in the twist tapered lattice is only for the E_{\perp} polarisation while that in the splay-bend we get it only E_{\parallel} polarisation. Here again, we find the diffraction pattern to change with the azimuth of the direction of the normal incidence of light with respect to the x axis. In particular for a direction of incidence along x-axis, E_{\parallel} mode only results in diffraction. When E is along y axis, i.e., for E_{\perp} , we find no diffraction whatsoever, since the medium is homogeneous for this state (see Figure 6.7(b)). In contrast, in a twist tapered lattice we find no diffraction for E_{\parallel} mode.

Bibliography

- [1] K. A. Suresh. , P. B. SunilKumar. and G. S. Ranganath., *Liq. Cryst.* **11** (1992) 73
- [2] K. Rokushima and J. Yamakita . , *J. Opt. Soc. Am.* **73** (1983) 901
- [3] K. A. Suresh., Yuvraj Sah., P.B. Sunil Kumar and G.S. Ranganath., *Physical Review Letters* **72** (1994) 2863
- [4] R. Mosseri and F.Bailly . , *J.Phys.I France*, **2** (1991) 1715
- [5] Y. Sah and G. S. Ranganath . , *Opt. Comm*, **114** (1995) 18

